Metal−Metal Bonding in $Rh_2(O_2CCF_3)_4$: Extensive Metal−Ligand Orbital Mixing Promoted by Filled Fluorine Orbitals

Dennis L. Lichtenberger,*,† John R. Pollard,† Matthew A. Lynn,† F. A. Cotton,‡ and Xuejun Feng‡

Contribution from the Department of Chemistry, The University of Arizona, Tucson, Arizona 85721-0041, and Laboratory for Molecular Structure and Bonding and Department of Chemistry, P.O. Box 300012, Texas A&M University, College Station, Texas 77842-3012

Received October 8, 1999

Abstract: He I and He II gas-phase photoelectron spectra of $Rh_2(O_2CCF_3)_4$ are reported. The electron configuration of the metal−metal bond of $Rh_2(O_2CCF_3)_4$ is determined to be $\sigma^2\,\pi^4\,\delta^2\,\delta^{*2}\,\pi^{*4}$ with an ionization energy order of $\sigma \approx \pi > \delta > \delta^* \approx \pi^*$. The δ^* and π^* ionization energies are similar within the range of vibrational energy separations. Assignment of the Rh−Rh δ ionization is assisted by previous observations that ionizations from δ orbitals in $M_2(O_2CCF_3)_4$ (M = Mo, W) and $Mo_2(O_2CH)_4$ show enhanced intensity over ionizations from the σ and π orbitals with He II excitation. Changes in ionization energies from the dimolybdenum molecule to the dirhodium molecule and changes in ionization intensities from He I to He II excitation indicate greater metal−ligand mixing in these molecules than observed in other dimetal tetracarboxylates. Amsterdam density functional calculations agree with the observation that the Rh−Rh δ^* and π^* energies are similar. The calculations also indicate substantial ligand mixing into the metal−metal σ and π orbitals, which is enhanced by the trifluoroacetate ligand despite the inductive withdrawal of electron density by the electronegative fluorine atoms. It is found that a specific set of ligand orbitals that possess the same symmetries as the Rh−Rh σ and π orbitals are destabilized by overlap interactions with the filled fluorine p orbitals, resulting in greater metal−ligand mixing among these orbitals. The increased mixing explains the long-observed enhancement of the δ and δ^* ionizations from He I to He II excitation for a number of $M_2(O_2CCF_3)_4$ (M = Mo, W, Ru) systems.

Introduction

Dirhodium molecules have a number of important applications in many areas of chemistry.[1] Most notably, many derivatives have proven to be valuable as catalysts for a variety of reaction processes including hydrogenation and dehydrogenation reactions,[2] oxidation and oxidative addition reactions,[3] photocatalytic reactions (water splitting),[4] and reactions involving carbenes.[5−8] Some dirhodium carboxylates have also been shown to possess relevant biological chemistry, such as antitumor activity.[9] In nearly all of these cases, the choice of ligand substituents on the dimetal species greatly affects the reactivity of the system. Also, the Rh−Rh bond is believed to be the site of reactivity in almost all of the catalytic studies. Therefore, it is valuable to understand the electronic structure of the Rh−Rh bond in these and similar complexes, and to examine how this interaction is affected by ligand substitution.

The orbital model of metal−metal bonding and antibonding interactions has given chemists a powerful tool to understand the structure and reactivity of dimetal systems. These orbitals, which are designated σ, π, δ, δ^*, π^*, and σ^*, possess different types of metal−metal and metal−ligand interactions that define the bonding and properties of these systems. The synthesis of new metal−metal bonded systems provides an opportunity for the experimental examination of the factors that influence their electronic structure, not only for the fundamental interest of the bonding in inorganic systems but also for the insight such work provides regarding the reactivity of these compounds. Such systems have now been prepared with a majority of the transition metals, thereby permitting study of these orbitals over a range of orbital electron occupations and metal−metal bond distances. The most direct method of probing the individual metal−metal electronic interactions is photoelectron spectroscopy, and this tool has provided much experimental information on the electronic structure of metal−metal bonds. Most of the initial photoelectron studies focused on Cr_2, Mo_2, and W_2 systems of the form $M_2(O_2CR)_4$,[10−21] but we have recently been able to

* To whom correspondence should be addressed.
† The University of Arizona.
‡ Texas A&M University.

(1) Cotton, F. A.; Walton, R. A. *Multiple Bonds Between Metal Atoms*; Clarendon Press: Oxford, 1993.
(2) Hui, B. C. Y.; Teo, W. K.; Rempel, G. L. *Inorg. Chem.* **1973**, *12*, 757−762.
(3) Shinoda, S.; Kojima, T.; Saito, Y. *J. Mol. Catal.* **1983**, *18*, 99.
(4) Sigal, I. S.; Mann, K. R.; Gray, H. B. *J. Am. Chem. Soc.* **1980**, *102*, 7252−7256.
(5) Doyle, M. P.; Shanklin, M. S. *Organometallics* **1994**, *13*, 1081−1088.
(6) Doyle, M. P.; Westrum, L. J.; Wolthuis, W. N. E.; See, M. M.; Boone, W. P.; Bagheri, V.; Pearson, M. M. *J. Am. Chem. Soc.* **1993**, *115*, 958−964.
(7) Doyle, M. P.; Bagheri, V.; Wandless, T. J.; Harn, N. K.; Brinkler, D. A.; Eagle, C. T.; Loh, K.-L. *J. Am. Chem. Soc.* **1990**, *112*, 1906−1912.
(8) Sheehan, S. M.; Padwa, A.; Snyder, J. P. *Tetrahedron Lett.* **1998**, *39*, 949−952.
(9) Hughes, R. G.; Bear, J. L.; Kimball, A. P. *Proc. Am. Assoc. Cancer Res.* **1972**, *13*, 120.
(10) Chisholm, M. H.; Clark, D. L.; Huffman, J. C.; Van der Sluys, W. G.; Kober, E. M.; Lichtenberger, D. L.; Bursten, B. E. *J. Am. Chem. Soc.* **1987**, *109*, 6796−6816.
(11) Lichtenberger, D. L.; Johnston, R. L. In *Metal−Metal Bonds and Clusters in Chemistry and Catalysis*; Fackler, J. P., Ed.: Plenum: 1989; pp 1−24.

10.1021/ja993618l CCC: $19.00
Published on Web 03/18/2000

study a much wider range of metal−metal bonded systems.[22−24] Unfortunately, dirhodium tetracarboxylates such as $Rh_2(O_2CCH_3)_4$ readily decompose thermally, making them unsuitable for study via gas-phase photoelectron spectroscopy. $Rh_2(O_2CCF_3)_4$ is the first dirhodium tetracarboxylate complex that has proven to be sufficiently thermally stable to study via gas-phase photoelectron spectroscopy.

It has been generally accepted that the formal metal−metal bond order in Rh(II)−Rh(II) carboxylates is one. This notion is supported by the vast amount of structural information reported on various $Rh_2(O_2CR)_4$ molecules in which all reported Rh−Rh bond distances are consistent with a single metal−metal bond.[1] The energetic ordering of the Rh−Rh bonding and antibonding orbitals is not as well substantiated. Starting from the ground-state configuration of $Mo_2(O_2CR)_4$, $\sigma^2\pi^4\delta^2$, the addition of six electrons as in $Rh_2(O_2CR)_4$ leads to a ground-state configuration of $\sigma^2\pi^4\delta^2\delta^{*2}\pi^{*}$,[4] assuming that the Rh−Rh π^* orbitals are destabilized relative to the δ^*.

As a result of this uncertainty, spectroscopic and computational work has been carried out to understand the valence electronic structure of these systems. The earliest studies were done by Dubicki and Martin,[25] who performed extended Hückel calculations on $Rh_2(O_2CH)_4$ and concluded the formal bond order to be one based on an electron configuration of $\sigma^2\pi^4\delta^2\delta^{*2}\pi^{*}$.[4] This report was followed by SCF-Xα calculations on $Rh_2(O_2CH)_4$ that indicated this same formal Rh−Rh bond order, but suggested that the δ^* orbital is destabilized relative to the π^* level, giving a ground-state configuration ordering of $\sigma^2\pi^4\delta^2\pi^{*4}\delta^{*2}$.[26,27] The switching of the Rh−Rh π^* and δ^* levels was attributed to the filled−filled symmetry interaction between the δ^* orbital and the appropriate symmetry combination of oxygen π-type lone pairs. The first direct experimental work came soon thereafter. EPR studies on $[Rh_2(O_2CCH_3)_4(H_2O)_2]^+$ ions showed that the unpaired electron occupies the π^* level.[28,29] This result was supported by a rigorous computational study (SCF-CI) where the unpaired electron for this species was determined computationally to be in the Rh−Rh π^* orbital.[30] However, other relatively high-level theoretical treatments have reported much different ground-state configurations. Ab initio calculations performed by Nakatsuji and coworkers suggest a ground-state Rh−Rh configuration of $\pi^4\delta^2\pi^{*4}\delta^{*2}\sigma^2$.[31] More recent SCF-Xα-SW calculations performed on the full $Rh_2(O_2CCF_3)_4$ molecule concur with the earlier Xα results by suggesting an orbital ordering of $\sigma^2\pi^4\delta^2\pi^{*4}\delta^{*2}$ with an energy separation between the δ^* and π^* orbitals of 0.48 eV and between their ionization energies of ∼0.75 eV.[32]

In this paper we report the photoelectron spectrum of $Rh_2(O_2CCF_3)_4$, the first dirhodium tetracarboxylate for which such data has been obtained. The assignment of this spectrum is aided by observation of the variations in ionization cross-sections with change of photon source and by comparison with the spectrum of $Mo_2(O_2CCF_3)_4$. Electronic structure calculations at several levels of sophistication (Fenske−Hall and density functional) are presented also. These results add important new understanding to the nature of the metal−metal interactions and how they are influenced by the perfluoroacetate ligand in $Rh_2(O_2CCF_3)_4$ as well as in $Mo_2(O_2CCF_3)_4$.

Experimental Section

Photoelectron Spectroscopy. Samples were prepared according to published procedures.[33] Pertinent instrument operating conditions have been discussed elsewhere.[24] During data collection, neither $Mo_2(O_2CCF_3)_4$ nor $Rh_2(O_2CCF_3)_4$ displayed any signs of decomposition. $Mo_2(O_2CCF_3)_4$ and $Rh_2(O_2CCF_3)_4$ exhibited sublimation temperatures (at 10^{-4} Torr) of 135−140 and 130−135 °C, respectively.

Calculations. Density functional calculations were performed with the ADF program developed by Baerends et al.[34] and vectorized by Ravenek.[35] The numerical integration procedure was developed by te Velde and co-workers.[36,37] The BLYP method was used for all calculations. The atomic orbitals on all centers were described by an uncontracted triple-ζ STO basis set (i.e., set IV) that is available with the ADF package. The $1s^2$ configuration on carbon, oxygen, and fluorine as well as the $1s^22s^22p^63s^23p^63d^{10}$ configuration on Rh and Mo were assigned to the core and treated by the frozen-core approximation. The molecular structures of $Mo_2(O_2CCH_3)_4$, $Mo_2(O_2CCF_3)_4$, and $Rh_2(O_2CCF_3)_4$ were fully optimized under the D_{2d} point group by appropriate orientation of the CF_3 groups. Pertinent geometric parameters with comparison to the crystallographically determined structures are presented in Table 1. The theoretically optimized structures for the molecules in the gas phase are generally in good agreement with the experimentally determined structures from single crystals, with the Mo−Mo distances 0.05−0.07 Å longer in the calculated structures. Calculations of the electronic structures and ionization energies were also carried out at the experimental geometries, and similar results were obtained. Only the results for which the ADF (BLYP) optimized geometries were employed are reported here.

Ionization energies can be determined in ADF by two methods. First, the orbital energies from the neutral ground-state calculation can be examined in a Koopmans-type approximation.[37,38] Second, the total

(12) Lichtenberger, D. L.; Blevins, C. H. *J. Am. Chem. Soc.* **1984**, *106*, 1636−1641.
(13) Lichtenberger, D. L.; Ray. C. D.; Stepniak, F.; Chen, Y.; Weaver, J. H. *J. Am. Chem. Soc.* **1992**, *114*, 10492−10497.
(14) Kober, E. M.; Lichtenberger, D. L. *J. Am. Chem. Soc.* **1985**, *107*, 7199−7201.
(15) Lichtenberger, D. L.; Kristofzski, J. G. *J. Am. Chem. Soc.* **1987**, *109*, 9, 3458−3459.
(16) Cotton, F. A.; Norman, J., J. R.; Stults, B. R.; Webb. T. R. *J. Coord. Chem.* **1976**, *5*, 217−223.
(17) Hillier, I. H.; Garner, C. D.; Mitcheson, G. R.; Guest, M. F. *J. Chem. Soc., Chem. Commun.* **1978**, 204−205.
(18) Coleman, A. W.; Green, J. C.; Hayes, A. J.; Seddon, E. A.; Lloyd, D. R.; Niwa, Y. *J. Chem. Soc., Dalton Trans.* **1979**, 1057−1064.
(19) Berry, M.; Garner, C. D.; Hillier, I. H.; MacDowell, A. A.; Walton, I. B. *Chem. Phys. Lett.* **1980**, *70*, 350−352.
(20) Atha, P. M.; Hillier, I. H.; Guest, M. F. *Mol. Phys.* **1982**, *46*, 437−448.
(21) Garner, C. D.; Hillier, I. H.; MacDowell, A. A.; Walton, I. B.; Guest, M. F. *J. Chem. Soc., Faraday Trans. 2* **1979**, *75*, 485−493.
(22) Lichtenberger, D. L.; Lynn, M. A.; Chisholm, M. H. 217th National Meeting of the American Chemical Society, Anaheim, CA, April 1999; American Chemical Society: Washington, DC., 1999; Abstract 027-INOR.
(23) Lichtenberger, D. L.; Lynn, M. A.; Chisholm, M. H.; 217th National Meeting of the American Chemical Society, Anaheim, CA, April 1999; American Chemical Society: Washington, DC, 1999; Abstract 253-INOR.
(24) Lichtenberger, D. L.; Lynn, M. A.; Chisholm, M. H. *J. Am. Chem. Soc.* **1999**, *121*, 12167−12176.
(25) Dubicki, L.; Martin, R. L. *Inorg. Chem.* **1970**, *9*, 673−675.
(26) Norman, J. G.; Kolari, H. J. *J. Am. Chem. Soc.* **1978**, *100*, 791−799.
(27) Bursten, B. E.; Cotton, F. A. *Inorg. Chem.* **1981**, *20*, 3042−3048.
(28) Kawamura, T.; Fukamachi, K.; Hayashida, S. *J. Chem. Soc., Chem. Commun.* **1979**, 945−946.
(29) Kawamura, T.; Fukamachi, K.; Sowa, T.; Hayashida, S.; Yonezawa, T. *J. Am. Chem. Soc.* **1981**, *103*, 364−369.
(30) Mougenot, P.; Demuynck, J.; Bernard, M. *Chem. Phys. Lett.* **1987**, *136*, 279−282.
(31) Nakatsuji, H.; Ushio, J.; Kanda, K.; Onishi, Y.; Kawamura, T.; Yonezawa, T. *Chem. Phys. Lett.* **1981**, *79*, 299−304.
(32) Cotton, F. A.; Dikarev, E. V.; Feng, X. *Inorg. Chim. Acta* **1995**, *237*, 19−26.
(33) Kitchens, J.; Bear, J. L. *Thermochim. Acta* **1970**, *1*, 537.
(34) Baerends, E. J.; Ellis, D. E.; Ros, P. *Chem. Phys.* **1973**, *2*, 41−51.
(35) Ravenek, W. *Algorithms and Applications on Vector and Parallel Computers*; te Riele, H., Dekker, T. J., van de Vorst, H. A., Eds.; Elsevier: Amsterdam, 1987.
(36) Boerrigter, P. M.; te Velde, G.; Baerends, E. J. *Int. J. Quantum Chem.* **1988**, *33*, 87−113.
(37) te Velde, G.; Baerends, E. J. *J. Comput. Phys.* **1992**, *99*, 84−98.
(38) Stowasser, R.; Hoffmann, R. *J. Am. Chem. Soc.* **1999**, *121*, 3414−3420.

Table 1. Structural Parameters from ADF Geometry Optimizations of $Mo_2(O_2CCH_3)_4$, $Mo_2(O_2CCF_3)_4$, and $Rh_2(O_2CCF_3)_4$ with Comparisons to Crystallographically Determined Structures[a]

	$Mo_2(O_2CCH_3)_4$		$Mo_2(O_2CCF_3)_4$		$Rh_2(O_2CCF_3)_4$	
	crystal[51]	ADF	crystal[52−54]	ADF	crystal[32,55]	ADF
M−M (Å)	2.089	2.160	2.114	2.170	2.390	2.442
M−O (Å)	2.114	2.116	2.115	2.116	2.028	2.104
M−M−O (°)	92.1	91.6	91.4	91.4	88.3	88
M−O−C (°)	117.7	115.9	115.6	116.2	117.5	117.2
O−C (Å)	1.273	1.283	1.256	1.280	1.250	1.271
O−C−C (°)	118.9	117.4	117.5	117.5	115.9	115.3
C−C (Å)	1.496	1.530	1.535	1.530	1.538	1.569
C−C−X (°) (X = H or F)	N/A	109.0, 109.4	111.3	110.0, 111.1	109.0	111.2, 108.9
C−X (Å) (X = H or F)	N/A	1.113, 1.094	1.295	1.357, 1.288	1.318	1.354, 1.364

[a] For the perfluoro systems, the crystallographic data reported here are an average of several crystal structures as referenced.

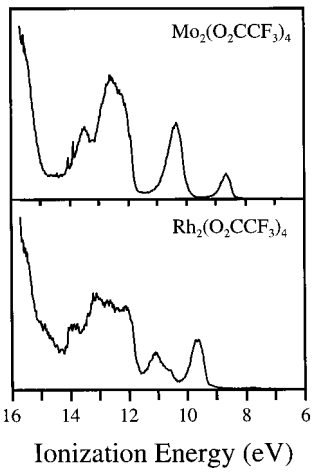

Figure 1. He I spectra (6−16 eV) of $Mo_2(O_2CCF_3)_4$ and $Rh_2(O_2CCF_3)_4$. The maximum number of counts in the spectra are 230 (M = Mo) and 1300 (M = Rh).

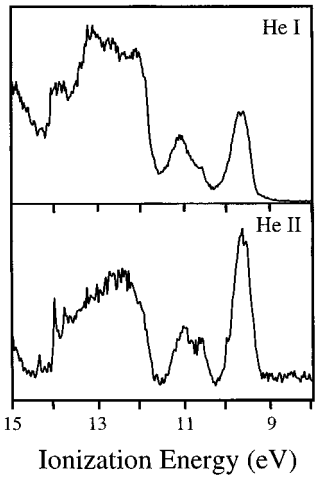

Figure 2. He I (2300 counts) and He II (450 counts) spectra (8−15 eV) of $Rh_2(O_2CCF_3)_4$.

energies of cations with a single electron removed from successive molecular orbitals (with the molecular geometry frozen) can be calculated and compared to the total energy of the neutral ground state of the system to determine successive vertical ionization energies. The energies obtained via this second method are termed ΔE_{SCF}. Although the Koopmans-type values have long been used to estimate ionization energies, it is the ΔE_{SCF} values that more correctly represent the ionization process because they account for the electron relaxation that occurs among the remaining electrons in a molecule once one electron has been removed. We have chosen to present both the Koopmans and ΔE_{SCF} values in the discussion that follows.

Fenske−Hall molecular orbital calculations have also been performed for comparison and for illustration of orbital distributions. Details of this method have been given previously.[39] The molecular structures employed are the same as obtained from the ADF calculations (i.e., the optimized structures).

Information from Ionization Features. Figure 1 shows the full He I spectrum of $Rh_2(O_2CCF_3)_4$ compared to that of $Mo_2(O_2CCF_3)_4$. $Mo_2(O_2CCF_3)_4$ has been studied extensively, as has $Mo_2(O_2CCH_3)_4$, and the ground-state electronic structure and photoelectron spectra of these molecules are perhaps the best understood of multiple metal−metal bonds.[18,19] In the spectra of $Mo_2(O_2CCF_3)_4$ and $Mo_2(O_2CCH_3)_4$, the band at lowest binding energy corresponds to the ionization of an electron from the Mo−Mo δ orbital.[12] The next lowest band results from the overlapping ionizations from the Mo−Mo σ and π-orbitals.[13,15] In the spectrum of $Mo_2(O_2CCF_3)_4$, a region of overlapping ionizations starting at about 11.75 eV has been attributed to primarily ligand-based orbitals (the sharp features at ∼14 eV in this spectrum arise from the Ar $^2P_{3/2}$ and $^2P_{1/2}$ ion states generated by the He Iβ line; Ar is present as an internal reference). The onset of overlapping ionizations at the same energy in the spectrum of $Rh_2(O_2CCF_3)_4$ is consistent with this interpretation, but the difference in the profiles of the bands from 12 to 14 eV suggests some changing interactions to be discussed later. As in the spectrum of $Mo_2(O_2CCF_3)_4$, the $Rh_2(O_2CCF_3)_4$ ionizations with energies less than 11.75 eV occur from orbitals that contain metal orbital character. More support is given to this assignment when the full He I and He II data for $Rh_2(O_2CCF_3)_4$, shown in Figure 2, are compared. The theoretical photoionization cross-section of the Rh 4d atomic orbital under He II ionization is predicted to increase when compared to that of the carbon, oxygen, and fluorine 2p atomic orbitals.[40] The features at ionization energies less than 11.75 eV grow substantially compared to those at higher energy, where ionizations are typically ligand-based, indicating that the former ionizations occur from orbitals that are high in rhodium character. Changes in the profile of the region above 11.75 eV from He I to He II excitation are more subtle, but are nonetheless significant for later discussion.

Figure 3 compares more closely the He I and He II photoelectron spectra of the metal-based region of $Rh_2(O_2CCF_3)_4$. The lowest ionization energy band at ∼9.60 eV is best fit with two asymmetric Gaussian peaks. The next two bands, which slightly overlap with each other, require only one Gaussian peak each. The fit parameters for these features in the photoelectron spectra of $Rh_2(O_2CCF_3)_4$ are summarized in Table 2.

In the He II spectrum there is a substantial increase in the area of peaks 1, 2, and 3 relative to peak 4, suggesting that the three ionizations at lowest energy arise from orbitals with a larger proportion of metal character. Because of the relative intensity and overall width of the band at lowest ionization energy, which contains peaks 1 and 2, and because of computational results to be discussed shortly, this feature is assigned to the ionizations of the Rh−Rh δ^* and π^* orbitals. The overall width of the band containing peaks 1 and 2 is 0.58 eV compared to the width of peak 3 which is 0.29 eV. The width of a band containing a single ionization is determined by the vibrational progression

(39) Lichtenberger, D. L.; Wright, L. L.; Gruhn, N. E.; Rempe, M. E. *Synth. Met.* **1993**, *59*, 353−367.

(40) Yeh, J. J.; Lindau, I. *At. Data Nucl. Data Tables* **1985**, *32*, 1−155.

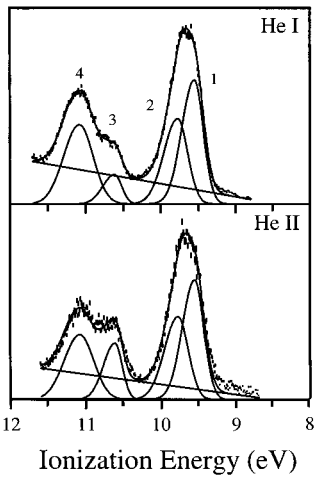

Figure 3. He I (1600 counts) and He II (700 counts) spectra (8−12 eV) of $Rh_2(O_2CCF_3)_4$.

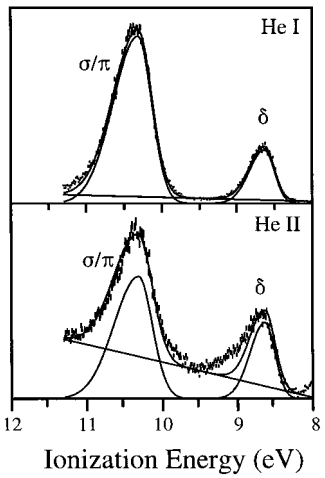

Figure 4. He I (1100 counts) and He II (400 counts) spectra (8−12 eV) of $Mo_2(O_2CCF_3)_4$.

Table 2. Peak Parameters for the He I and He II Photoelectron Spectra of $Mo_2(O_2CCF_3)_4$ and $Rh_2(O_2CCF_3)_4$ [a]

band	ionization energy (eV)	He I width high/low (eV)	area He I	area He II	origin
		$Mo_2(O_2CCF_3)_4$			
δ	8.63	0.48/0.30	0.21	0.40	δ
$\sigma + \pi$	10.32	0.77/0.43	1	1	$\sigma + \pi$
		$Rh_2(O_2CCF_3)_4$			
1	9.55	0.39/0.28	1.17	1.36	$\pi^* + \delta^*$
2	9.77	0.43/0.31	0.88	1.04	
3	10.61	0.36/0.22	0.24	0.56	δ
4	11.08	0.48/0.43	1	1	$\sigma + \pi$

[a] Peak areas for the Mo system are relative to that of the ($\sigma + \pi$) band and for the Rh system are relative to that of peak 4.

associated with excitation to the positive ion state. If the orbital from which the electron is removed is substantially bonding, the vibrational progression will be relatively broad. Assuming similar widths for the unresolved vibrational progressions of peaks 1, 2, and 3, the overall width of the first band indicates peaks 1 and 2 may be separated by as much as 0.2 eV. Since the vibrational widths of these peaks are greater than 0.2 eV, the vibrational progressions of 1 and 2 are merged, and separate peaks are not observed in the first band. It is only possible to say that the δ^* and π^* ionization energies are similar within the spread of vibrational energies with excitation.

As for the Rh−Rh σ, π, and δ ionizations, information from previous studies is particularly helpful. For systems such as $Mo_2(O_2CCF_3)_4$,[18,19] $W_2(O_2CCF_3)_4$,[41] and $Ru_2(O_2CCF_3)_4$,[42,43] it has been observed that in a He II spectrum, the δ ionization approximately doubles in intensity relative to the σ and π ionizations as compared to the He I spectrum. Because of the similar increase in intensity observed here for peak 3 relative to peak 4, peak 3 is attributed to the Rh−Rh δ ionization and peak 4 to the Rh−Rh σ and π ionizations. The band at 11.08 eV can also be assigned as arising from ionizations from Rh−Rh σ- and π-containing orbitals because of its location, which correlates with the analogous band in the spectra of $Mo_2(O_2CCF_3)_4$ (10.44 eV) and $Ru_2(O_2CCF_3)_4$ (10.41 eV).

The enhanced intensity in the He II experiment of the δ ionization as compared to the σ and π ionizations has been reproduced here for $Mo_2(O_2CCF_3)_4$. Figure 4 shows the He I/He II comparison for these features and fit parameters for these spectra are presented in Table 2. With He II ionization, the δ ionization feature doubles in intensity relative to that of the $\sigma + \pi$ band. This phenomenon has been used as a fingerprint for the identity of metal−metal δ and δ^* ionizations for this and other systems.[18,42−44] The exact cause of this cross-section phenomenon for the δ ionization has so far not been explained. It has been observed only in the bridging dimetal acetates and has been thought to be related to the unique nodal properties of the δ bond as well as to the electron-withdrawing ability of the bridging ligands (which directly relates to the ionization energy of the metal−metal orbitals). The enhancement was first noticed by Green and co-workers who reported the He I and He II spectra for a series of quadruply bonded molybdenum complexes, $Mo_2(O_2CCH_3)_4$, $Mo_2(O_2CC(CH_3)_3)_4$, $Mo_2(O_2CCF_3)_4$, and $Mo_2(O_2CH)_4$.[18] For this series, it was observed that the He II intensity of the δ-ionization grew substantially relative to the $\sigma + \pi$ ionizations for both $Mo_2(O_2CH)_4$ (($\sigma + \pi$):δ ratio goes from 5:1 to 2.5:1) and $Mo_2(O_2CCF_3)_4$ (($\sigma + \pi$):δ ratio goes from 3:1 to 1.7:1). They reported a small intensity enhancement for the δ-band of $Mo_2(O_2CCH_3)_4$ and an even smaller one for $Mo_2(O_2CC(CH_3)_3)_4$. Green and co-workers later used this enhancement to assign the photoelectron spectrum of $Ru_2(O_2CCF_3)_4$,[42,43] and again observed it in recent synchrotron studies reported for $Mo_2(O_2CCF_3)_4$.[44] We have also observed this enhancement of the δ ionization band for $W_2(O_2CCF_3)_4$ but did not see an appreciable enhancement for $W_2(O_2CCH_3)_4$.[41] For the ruthenium system, it was suggested that because the $\sigma + \pi$ band had an IP (10.41 eV) similar to that of the analogous molybdenum compound (10.44 eV), these orbitals may contain a relatively large amount of carboxylate character. This hypothesis also explains the intensity changes for the δ and $\sigma + \pi$ bands for both systems. The mixing of carboxylate character into the σ and π ionizations will be a point for consideration.

It is difficult to determine whether the Rh−Rh δ^* ionization feature exhibits the same increase in intensity as the δ band because of the substantial overlap of this feature with that of the Rh−Rh π^* ionization envelope. Green and co-workers observed separate δ^* and π^* ionization features in the photoelectron spectrum of $Ru_2(O_2CCF_3)_4$,[43] for which the electronic ground state is $\delta^{*2}\pi^{*2}$, with the assumption that these features represent ionizations from distinct molecular orbitals for this paramagnetic system. However, $Ru_2(DtolF)_4$ (DtolF = *N*,*N*′-di-*p*-tolylformamidinate; also termed DFM and *p*-CH_3-form) has been shown to be diamagnetic and must therefore have an electronic occupation of $\pi^{*4}\delta^{*0}$.[45] The ordering of the M−M δ^* and π^* orbitals depends on the amount of ligand character in the δ^* orbital, such that strongly donating ligands with orbitals of the appropriate symmetry tend to destabilize the M−M δ^* orbital above the M−M π^* orbital. This phenomenon has been discussed elsewhere[32,45] and will be reviewed briefly in the computational results section.

Therefore, based on this photoelectron data the ground-state electron configuration of the Rh−Rh bond in $Rh_2(O_2CCF_3)_4$ is $\sigma^2\pi^4\delta^2\delta^{*2}\pi^{*4}$ with the ionizations from the δ^* and π^* orbitals being very close in

(41) Blevins, C. H., II. *Diss. Abstr. Int. B* **1984**, *45*, 1186.
(42) Clark, D. L.; Green, J. C.; Redfern, C. M.; Quelch, G. E.; Hillier, I., H.; Guest, M. F. *Chem. Phys. Lett.* **1989**, *154*, 326−329.
(43) Clark, D. L.; Green, J. C.; Redfern, C. M. *J. Chem. Soc., Dalton Trans.* **1989**, 1037−1044.
(44) Brennan, J.; Cooper, G.; Green, J. C.; Payne, M. P.; Redfern, C. M. *J. Electron Spectrosc. Relat. Phenom.* **1995**, *73*, 157−162.
(45) Cotton, F. A.; Ren, T. *Inorg. Chem.* **1991**, *30*, 3675−3679.

energy. The observation that the δ^* and π^* ionizations are merged in the same energy region largely obviates the question of which is the more stable positive ion state. The δ ionization is clearly observed to precede the σ and π ionization band. According to the differences in the He I and He II spectra of $Rh_2(O_2CCF_3)_4$, it appears that the Rh−Rh σ and π bonding molecular orbitals contain a considerable amount of ligand character. Similarly, some rhodium character is suggested by subtle changes in the predominantly ligand region between 13 and 14 eV compared to the spectrum of $Mo_2(O_2CCF_3)_4$ and by the He I/He II comparison of this region. This matter will be addressed shortly.

Information from Calculations

Before discussing the results of the calculations, it is important to clarify the language for describing the orbital structure of molecules with metal−metal bonds. The molecular orbitals with predominant metal d orbital character (and the associated ionizations) are labeled with the traditional Greek symbols σ, π, δ, δ^*, etc. of a dimetal unit. These molecular orbitals may also contain a substantial amount of ligand character, and this metal−ligand mixing is important to understanding the electronic structure and properties of these molecules. Under the D_{4h} point group, the δ and δ^* orbitals refer to the combinations of the metal d_{xy} orbitals while the $d_{x^2-y^2}$ orbitals are primarily involved in σ bonding to the ligands. The molecular orbitals with predominant ligand character are labeled with group theoretical symbols, using the D_{4h} symmetry of the atoms directly bonded to the metals. For interactions between the dimetal unit and the ligands it is helpful to remember the symmetries of the metal−metal orbitals. Thus the metal−metal σ orbital may mix with the ligand a_{1g} combinations, the metal−metal π orbitals may mix with the ligand e_u orbitals, and so on. These interactions are the focus of the discussion.

$Rh_2(O_2CCF_3)_4$ has been examined previously via the SCF-Xα-SW method.[32] This calculation found a number of ligand-based orbitals in the same energy region as the Rh−Rh δ^*, π^*, and δ levels. The ground-state calculation of this system indicated that the HOMO of $Rh_2(O_2CCF_3)_4$ is the Rh−Rh δ^* orbital and that it is separated from the next highest occupied molecular orbital, the Rh−Rh π^* orbital, by 0.48 eV. The calculated ionization energies, however, suggested that a ligand-based ionization of e_u symmetry should occur (12.21 eV) between the Rh−Rh δ^* (11.99 eV) and π^* (12.78 eV) ionizations. A second ligand-based ionization (a_{1g} symmetry) was calculated to be at nearly the same energy as that of the π^* and yet another (b_{1g} symmetry) was calculated to be at higher ionization energy than the Rh−Rh δ bond. In the computational comparison of $Rh_2(O_2CH)_4$ and $Rh_2(O_2CCF_3)_4$, there was a different ordering of the ligand-based orbitals between the formate and trifluoroacetate ligand set. It was noted that the e_u set of orbitals of $Rh_2(O_2CCF_3)_4$ contained C−C bonding character and that there was considerable contribution from the fluorine atoms. This note will become important. In addition, Fenske−Hall calculations presented in this same report agreed with the SCF-Xα-SW results in that the third highest occupied orbital was a ligand-based orbital of e_u symmetry that contained C−C bonding character.

The experimental and computational results to this point present some unexpected observations for the $M_2(O_2CCF_3)_4$ molecules in general and the $Rh_2(O_2CCF_3)_4$ molecule in particular. Basically, the strongly electron-withdrawing CF_3 groups are expected to stabilize the orbital energies of $(O_2CCF_3)^-$ in comparison to those of $(O_2CCH_3)^-$ and to pull them away from the valence metal orbitals. However, the ionization studies indicate that the valence σ and π ionizations of $Mo_2(O_2CCF_3)_4$ are associated with more ligand character than are those of $Mo_2(O_2CCH_3)_4$, and the SCF-Xα calculation on $Rh_2(O_2CCF_3)_4$ intermingles metal- and ligand-based ionizations in the low-energy region.

Table 3. Summary of Energies and Orbital Compositions of $Rh_2(O_2CCF_3)_4$ Determined via the Fenske−Hall Method[a]

orbital energy (eV)	orbital symmetry	amount of metal character
−10.16	b_{1u}	91% Rh−Rh π^*
−10.30	e_g	77% Rh−Rh δ^*
−12.10	e_u	10% Rh−Rh π
−12.33	b_{2g}	87% Rh−Rh δ (d_{xy})
−12.51	a_{1g}	24% Rh−Rh σ
−13.53	e_u	90% Rh−Rh π
−14.24	b_{1g}	22% Rh−Rh δ ($d_{x^2-y^2}$)
−15.75	a_{1g}	80% Rh−Rh σ

[a] Symmetry labels are for the D_{4h} point group. Three ligand-based orbitals at ∼−15.5 eV have been omitted from this table.

Table 4. Summary of Energies and Orbital Compositions of $Mo_2(O_2CCH_3)_4$ and $Mo_2(O_2CCF_3)_4$ Determined via the Fenske−Hall Method[a]

orbital energy (eV)	orbital symmetry	amount of metal character
	$Mo_2(O_2CCH_3)_4$	
−7.23	b_{2g}	89% Mo−Mo δ
−10.33	e_u	89% Mo−Mo π
−11.49	a_{1g}	78% Mo−Mo σ
	$Mo_2(O_2CCF_3)_4$	
−9.17	b_{2g}	86% Mo−Mo δ (d_{xy})
−11.74	e_u	83% Mo−Mo π
−12.34	e_u	16% Mo−Mo π
−12.35	a_{1g}	44% Mo−Mo σ
−13.67	b_{1g}	13% Mo−Mo δ ($d_{x^2-y^2}$)
−14.24	a_{1g}	62% Mo−Mo σ

[a] Symmetry labels are for the D_{4h} point group.

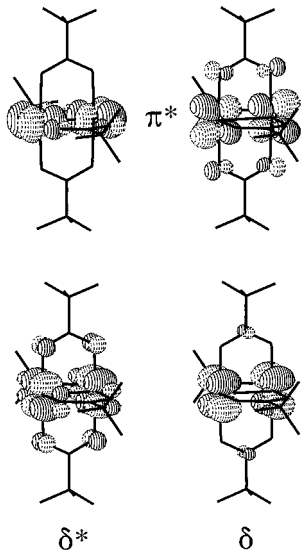

Figure 5. Contour plots (value ±0.05) of the Rh−Rh π^*, δ^*, and δ molecular orbitals.

Orbital Energies and Interactions. Closer examination of Fenske−Hall calculations on several dimetal tetraacetate molecules and on the isolated ligands helps to clarify the fragment orbital interactions within the ligand and with the metals. Orbital energies and characters for $Mo_2(O_2CCH_3)_4$, $Mo_2(O_2CCF_3)_4$, and $Rh_2(O_2CCF_3)_4$ are summarized in Tables 3 and 4. Contour plots of the highest occupied molecular orbitals (Rh−Rh π^*, δ^*, and δ) of $Rh_2(O_2CCF_3)_4$ are shown in Figure 5. The ordering of molecular orbitals found with this method agrees almost identically with that using the SCF-Xα-SW method. One

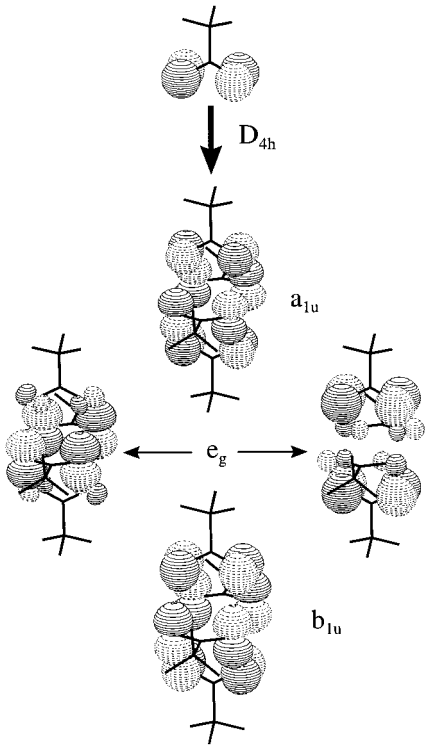

Figure 6. Contour plots (value ±0.05) of the antisymmetric combination of oxygen $2p_\perp$ orbitals and the four linear combinations (a_{1u}, b_{1u}, and e_g) of this orbital that are formed under a paddlewheel geometry.

difference is that this Fenske−Hall calculation places three ligand-based molecular orbitals between the ligand-based b_{1g} orbital and the Rh−Rh σ bond, while the SCF-Xα-SW results placed two ligand-based orbitals in this same region. The previously reported molecular orbital energies and compositions are also similar to those found here.

The two highest occupied orbitals of $Rh_2(O_2CCF_3)_4$ in this calculation are the Rh−Rh δ* and π*, which are separated by 0.14 eV. The similarity in energy of these two orbitals follows from the effect of the metal−metal single bond distance and from the different ligand contributions to the δ* and π* orbitals. To a first approximation, the M−M δ* orbital is the least antibonding of the metal−metal antibonding orbitals (i.e., the δ*, π*, and σ* orbitals) because of the smaller overlap between the d_{xy} atomic orbitals on the metal centers. One of the highest occupied orbitals of the trifluoroacetate ligand is an antisymmetric combination of the oxygen $p_\perp$ atomic orbitals. Under D_{4h} symmetry, this fragment orbital forms linear combinations of a_{1u}, b_{1u}, and e_g symmetry, as shown in Figure 6. The b_{1u} combination has the appropriate symmetry and orbital orientation to combine with the Rh−Rh δ* fragment orbital to form one molecular orbital that is metal−ligand bonding as well as one that is metal−ligand antibonding. The metal−ligand antibonding combination of these fragment orbitals is the molecular orbital that is ordinarily called the Rh−Rh δ* orbital. As shown in Table 3, the orbital labeled Rh−Rh δ* is 77% metal in character. The other 23% of the orbital character is from the oxygen $p_\perp$ orbitals of the ligands. The oxygen $p_\perp$ character in this orbital is apparent from the contour plot in Figure 5. As a result of the metal−ligand antibonding nature of this orbital, the Rh−Rh δ* orbital is destabilized.

The ligand character in the δ* molecular orbital, as shown in Table 3 and illustrated in Figure 5, is calculated to be more than twice that in the π* orbital. In the Rh−Rh π* orbital this ligand character, which is composed of the second highest

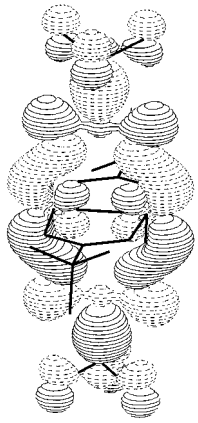

Figure 7. Contour plot (value ±0.05) of the ligand-based, Rh−Rh π-containing (e_u) molecular orbital.

occupied orbital of the trifluoroacetate ligand (to be discussed below), is antibonding with respect to the Rh−Rh π* orbital. Such an interaction acts to destabilize this metal-based orbital. As for the relative metal−metal antibonding character of the π* orbital in $Rh_2(O_2CCF_3)_4$, it is certainly less than that of the π* orbital in a system possessing a metal−metal quadruple, triple, or double bond because of the relatively longer metal−metal bond distance observed in this Rh−Rh single bond-containing system. The π* orbital is expected to be slightly more metal−metal antibonding than the δ* orbital, but the δ* orbital is more metal−ligand antibonding than the π* orbital. These interactions tend to compensate, and the Fenske−Hall calculation determines that the Rh−Rh δ* and π* orbitals are nearly degenerate for $Rh_2(O_2CCF_3)_4$.

The O−C−O π-bonding and π-antibonding fragment orbitals form combinations of a_{2g}, e_u, and b_{2g} symmetry, the last of which can form bonding and antibonding combinations with the Rh−Rh δ bond.[24] As seen from the contour plot of the Rh−Rh δ bond in Figure 5, there is very little ligand character in this orbital. The oxygen character is canceled out because of the similar amount of O−C−O π-bonding and π-antibonding b_{2g} symmetry fragment orbitals that contribute to this molecular orbital, leaving a small amount of carbon character in the Rh−Rh δ bond.

As with the SCF-Xα-SW calculations, the Fenske−Hall calculations suggest that there should be numerous ligand-based, metal−metal bond-containing ionizations throughout the metal-based ionization manifold for both perfluoroacetate molecules. The ligand-based molecular orbitals for $Rh_2(O_2CCF_3)_4$ in the outer valence region are a doubly degenerate e_u set located at −12.10 eV and a singly degenerate a_{1g} orbital at −12.51 eV. A contour plot of one of the e_u orbitals is presented in Figure 7. These e_u orbitals contain 10% Rh−Rh π-bonding character but the electron density of these molecular orbitals is predominantly located on the oxygen atoms and throughout the ligands. Likewise, the a_{1g} orbital at −12.51 eV possesses a small amount of Rh−Rh σ-bonding character with the remainder of the density found at the oxygen and fluorine atoms. These orbitals have also been found in theoretical treatments of $Rh_2(O_2CH)_4$, but they have considerably different ligand character and are both more stable than the Rh−Rh δ orbital, unlike for $Rh_2(O_2CCF_3)_4$ for which calculations suggest that the ligand-based e_u orbital should be less stable than this metal−metal bonding orbital. In further contrast, as seen in Table 4, the three highest occupied molecular orbitals of the acetate system $Mo_2(O_2CCH_3)_4$ are metal-based. A stepwise examination of the fragment orbitals

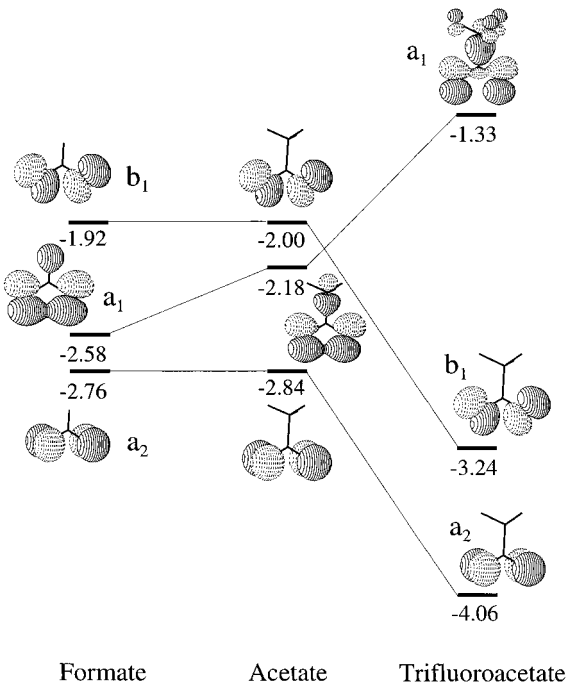

Figure 8. Correlation diagram of highest occupied orbitals (contour value ±0.05) of the formate, acetate, and trifluoroacetate ligands. One of the deeper orbitals of each ligand is included to show the correlation to the HOMO of trifluoroacetate. Energies are in eV and symmetry labels are for the C_{2v} point group.

of these ligands is therefore necessary to understand how they interact differently with the metal−metal bonding manifold.

Ligand Valence Orbitals. For the purposes of this correlation, the formate ($^{-}O_2CH$), acetate ($^{-}O_2CCH_3$), and trifluoroacetate ($^{-}O_2CCF_3$) ligands will be compared. A correlation diagram of some of the highest occupied molecular orbitals of each of these ligands, as determined by the Fenske−Hall method, is presented in Figure 8. Analogous calculations were performed via ADF and similar results were obtained. The highest occupied orbital of the formate ligand is calculated to be an in-plane, antisymmetric (b_1 symmetry) combination of oxygen 2p atomic orbitals. The next highest occupied orbital is composed of an in-plane, symmetric (a_1) combination of oxygen 2p orbitals that are out-of-phase with the orbital character on the H atom. The third highest occupied orbital is an out-of-plane, antisymmetric (a_2) combination of oxygen 2p AOs. Similar orbitals occur for the acetate ligand with the exception that the a_1 orbital is less stable because of the increased O−C antibonding interaction. All of these orbitals exist for the trifluoroacetate, but there is an important difference that occurs as a result of the fluorine lone pairs: the HOMO of the trifluoroacetate ligand is not the same as for the acetate or formate ligands. Because of the electron-withdrawing capability of the fluorine atoms, the b_1 and a_2 valence orbitals of trifluoroacetate are more stable than in the formate or acetate ligands. However, as a result of the lone pairs of the fluorine atoms, the a_1 orbital contains additional antibonding character between the fluorine atoms and the C−C σ bond. This orbital is calculated to be in the same energy vicinity as the HOMOs of the formate and acetate ligands. Furthermore, in addition to the C−C σ-bonding and C−F antibonding character of this orbital, there is calculated to be a considerable amount of oxygen character that is oriented such that it can interact in a σ fashion with the metal atoms of a metal−metal bonded system.

This orbital overlap effect of the fluorine p orbitals on these ligand orbitals is reminiscent of the "mesomeric" effect of fluorine p orbitals on benzene π electrons in fluorobenzenes[46,47] or the "hyperconjugative" effect of C−H or C-heteroatom bonds on adjacent carbon p orbitals.[47] In the fluorobenzenes the stabilization provided by the inductive electron withdrawal by the fluorine on the first benzene π ionization is countered by the filled−filled interaction between the fluorine p_π electrons and the benzene π electrons. In contrast to traditional examples of hyperconjugation, the effect observed for fluorination of the acetate ligand involves neither C-heteroatom bonds nor carbon p_π orbitals. Instead, the special feature for the fluorination of the acetate ligand is that the p orbital electrons ("lone pairs") of the three fluorines have filled−filled interactions with the carbon−carbon σ bond. This bond in turn has a filled−filled interaction with the in-plane symmetric combination of the oxygen p electrons. The highest occupied orbital is the antibonding combination composed of these fluorine p orbitals, the carbon−carbon bond, and the in-plane oxygen p orbitals as pictured in Figure 8. In this case the stabilization provided by the inductive electron withdrawal by the fluorine atoms is countered by the filled-filled interaction between the p orbital electrons of the three fluorine atoms and the carbon−carbon σ bond.

When four trifluoroacetate ligands are placed in a paddle-wheel orientation around two metal centers, this highest occupied molecular orbital forms linear combinations with symmetries (under the D_{4h} point group) of a_{1g}, e_u, and b_{1g} which are the same, respectively, as the M−M σ and π bonds and the δ combination of the M $d_{x^2-y^2}$ orbitals. Of course, these ligand fragment orbitals can form bonding and antibonding combinations with the metal fragment orbital of appropriate symmetry. Because the δ combination of the M $d_{x^2-y^2}$ orbitals is empty, only the metal−ligand bonding combination is occupied. For this reason, this b_{1g} combination is the most stable of the four ligand-based orbitals shown in Table 3. Likewise, because the Rh−Rh σ and π bonds are occupied, as are the three remaining combinations of the trifluoroacetate HOMO, the a_{1g} and e_u molecular orbitals can have substantial mixing between the metal and the ligands. The mixing of the e_u combination with the Rh−Rh π bond is shown in Figure 7.

Metal−Ligand Interactions. A molecular orbital diagram that summarizes all of these various metal−ligand interactions is presented in Figure 9. This diagram is based on the results of the current Fenske−Hall calculation and the energies are not those that have been determined experimentally, although there are many similarities. For instance, the order of the valence orbitals from the Fenske−Hall calculation is the same as seen experimentally from the spectrum of $Rh_2(O_2CCF_3)_4$, with the exception that the δ orbital is placed slightly below the first π orbital. The major metal−ligand interactions are those that involve the Rh−Rh σ, π, π^*, and δ^* orbitals. The δ^* orbital is metal-based, but contains some amount of metal−ligand antibonding character. In the absence of the ligand set, the δ^* fragment orbital is considerably more stable than the Rh−Rh π^* fragment orbital, but upon mixing with the ligands, the δ^* orbital becomes similar in energy to the Rh−Rh π^* orbital. As for the Rh−Rh δ bond, it is slightly destabilized from its energy in the Rh_2^{4+} fragment because of a slight excess of the ligand b_{2g} O−C−O π-bonding fragment orbital over the π-antibonding ligand fragment orbital of the same symmetry. Regarding the

(46) Brundle, C. R.; Baker, A. D. *Electron Spectroscopy: Theory, Techniques and Applications*; Academic Press: London, 1977.

(47) Briggs, D. *Handbook of X-ray and Ultraviolet Photoelectron Spectroscopy*; Heyden: London, 1977.

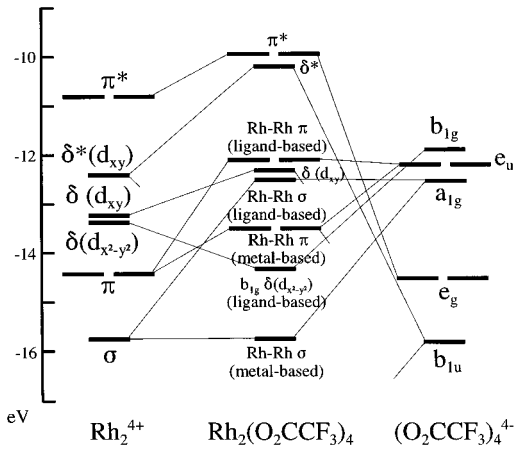

Figure 9. Molecular orbital diagram of $Rh_2(O_2CCF_3)_4$ from a transformed Fenske−Hall calculation. All orbitals in this diagram are occupied. For clarity, the levels of the degenerate δ (d_{xy}) and δ ($d_{x^2-y^2}$) Rh_2^{4+} fragment orbitals have been staggered. If the molecular orbital energies had been taken from the experimentally determined energies, the δ (d_{xy}) orbital would be located above the ligand-based Rh−Rh π orbitals.

Rh−Rh σ and π bonds, these fragment orbitals are more stable than are the appropriate symmetry combinations of the trifluoroacetate orbitals in the Fenske−Hall calculation. Therefore, the less stable (i.e., antibonding) combination of these ligand and metal fragment orbitals are ligand-based in the Fenske−Hall and SCF-Xα-SW calculations.

The primary point is that the metal−metal σ and π orbitals can mix with filled trifluoroacetate orbitals of the same symmetry. The calculated order of the ionizations, the primary ligand or metal character in the least stable e_u and a_{1g} orbitals, and the degree of metal−ligand mixing are sensitive to the relative energies of the metal−metal and ligand fragment orbitals. The photoelectron spectroscopy indicates that there is substantial metal−ligand mixing in the σ and π ionizations. The SCF-Xα and Fenske−Hall calculations seem to place these ligand orbitals somewhat too unstable relative to the metal orbitals, although it must be emphasized that such results are for the ground-state ordering of these orbitals rather than the energetic order in which electrons are photoionized from these orbitals.

Such a molecular orbital diagram also explains the change that occurs in the ionization profile in the 12−14 eV region. The ionization intensity near 12 eV appears to increase in the He II spectrum relative to the ionizations at higher ionization. Assuming that the ionizations with some metal-based σ and π character are in this area, these features would indeed be expected to increase in intensity in the He II experiment. Because of the large number of overlapping ionizations that occur in this part of the spectrum, it is difficult to make these assignments conclusively, but such a result is consistent with the remainder of the spectrum as well as with these calculations.

Ionization Energies. Density functional theory has been used previously to probe metal−metal bonds,[24,48−50] and the ability of ADF to calculate ionization energies for the systems that have been studied has been reasonably good. ADF computational results are consistent with the band assignments for the photoelectron spectrum of $Mo_2(O_2CCF_3)_4$ as shown in Table 5. The ionization energies determined with the ADF package (BLYP method) via the Koopmans and ΔE_{SCF} methods for the highest metal-containing orbitals of $Rh_2(O_2CCF_3)_4$ are also presented in Table 5. There are several interesting comparisons that can be made between the results from the ADF and Fenske−Hall methods. ADF finds that the Rh−Rh δ* orbital is slightly less stable than the π* orbital, while the Fenske−Hall calculation inverts the order of these two orbitals, but both methods determine that they are within 0.2 eV, in agreement with analysis of the photoelectron spectrum. In the ADF calculation, the separation between the Koopmans values for the δ* and π* orbitals is calculated to be 0.08 eV, whereas the ΔE_{SCF} value is 0.17 eV. In the Fenske−Hall calculations, these orbitals are separated by 0.14 eV. Further, the ADF Koopmans energies suggest that the orbitals that follow the Rh−Rh δ orbital to higher binding energy contain Rh−Rh σ and π character and are metal-based in the neutral ground-state calculation but are ligand-based in the cation calculation. As is evident from Table 5, relaxation of the Rh−Rh σ- and π-containing orbitals upon photoionization introduces a large amount of ligand character into these orbitals, whereas the change in the amount of metal character in the δ and δ* orbitals is much smaller. In fact the relaxation is such that for $Rh_2(O_2CCF_3)_4$, the Rh−Rh σ- and π-containing orbitals change from predominantly metal-based in the neutral molecule (69 and 66% Rh, respectively) to ligand-based (27 and 36% Rh) in the respective cation states. A similar trend is observed for $Mo_2(O_2CCF_3)_4$, although the Mo−Mo σ and π orbitals are calculated to contain more metal character in the cation states (65 and 64%, respectively) than in the analogous rhodium system because the molybdenum d orbitals are inherently less stable than the Rh d orbitals. The intensity of the σ and π bands would therefore be expected to decrease relative

Table 5. Ionization Energies and Orbital Compositions Calculated with the ADF Package Using the BLYP Method for $Mo_2(O_2CCH_3)_4$, $Mo_2(O_2CCF_3)_4$, and $Rh_2(O_2CCF_3)_4$ [a]

expt IP (eV)	ΔE_{SCF} IP (eV)	Koopmans IP (eV)	orbital character: neutral	orbital character: cation
		$Mo_2(O_2CCH_3)_4$		
6.89	6.89	6.89	77% Mo−Mo δ	78% Mo−Mo δ
8.68	8.38	8.34	85% Mo−Mo π	62% Mo−Mo π
	8.65	8.46	87% Mo−Mo σ	68% Mo−Mo σ
shift	0.09	2.64		
		$Mo_2(O_2CCF_3)_4$		
8.76	8.76	8.76	74% Mo−Mo δ	78% Mo−Mo δ
10.46	10.02	9.96	85% Mo−Mo π	64% Mo−Mo π
	10.28	10.09	88% Mo−Mo σ	65% Mo−Mo σ
shift	0.20	2.65		
		$Rh_2(O_2CCF_3)_4$		
9.55−9.77	9.55	9.55	74% Rh−Rh δ*	64% Rh−Rh δ*
	9.72	9.63	88% Rh−Rh π*	73% Rh−Rh π*
10.61	10.72	10.65	85% Rh−Rh δ	80% Rh−Rh δ
11.08	10.61	10.94	66% Rh−Rh π	36% Rh−Rh π
	11.46	11.97	69% Rh−Rh σ	27% Rh−Rh σ
∼12.0	11.49	12.06	25% Rh−Rh π	53% Rh−Rh π
shift	0.27	2.80		

[a] All calculated energies have been shifted by the amount indicated so that the first ionization matches the experimental value.

(48) Ziegler, T. *J. Am. Chem. Soc.* **1985**, *107*, 4453−4459.
(49) Cotton, F. A.; Feng, X. *J. Am. Chem. Soc.* **1997**, *119*, 7514−7520.
(50) Cotton, F. A.; Feng, X. *J. Am. Chem. Soc.* **1998**, *120*, 3387−3397.
(51) Hino, K.; Saito, Y.; Benard, M. *Acta Crystallogr., Sect. B* **1981**, *37*, 2164.
(52) Ouyang, X.; Campana, C.; Dunbar, K. R. *Inorg. Chem.* **1996**, *35*, 7188−7189.
(53) Campana, C.; Dunbar, K. R.; Ouyang, X. *J. Chem. Soc., Chem. Commun.* **1996**, 2427−2428.
(54) Handa, M.; Sono, H.; Lasamatsu, K.; Kasuga, K.; Mikuriya, M.; Ikenoue, S. *Chem. Lett.* **1992**, 453−456.
(55) Cotton, F. A.; Kim, Y. *Eur. J. Solid State Inorg. Chem.* **1994**, *31*, 525−534.

to that of the δ band from He I to He II excitation as is indeed observed in the spectra of $Mo_2(O_2CCF_3)_4$ and $Rh_2(O_2CCF_3)_4$. The δ^* and π^* orbital characters are intermediate in nature and show intermediate changes in He I/He II intensities.

The amount of ligand character that is added to the Mo−Mo σ and π orbitals of $Mo_2(O_2CCH_3)_4$ is calculated to be similar to that for $Mo_2(O_2CCF_3)_4$. As is shown in Table 5, the Mo−Mo σ and π orbitals remain predominantly metal-based (68 and 62%, respectively). The result is that the intensity of the δ ionization band may be enhanced for all of these compounds, but it is expected to be more enhanced for $Rh_2(O_2CCF_3)_4$ than for $Mo_2(O_2CCF_3)_4$ and $Mo_2(O_2CCH_3)_4$. The relative peak areas presented in Tables 1 and 2 for the trifluoracetates and found by Green and co-workers[18] for $Mo_2(O_2CCH_3)_4$ (($\sigma + \pi$):δ for He I is 1:0.21 and for He II is 1:0.36) support this conclusion. The a_{1g} and e_u trifluoroacetate-based fragment orbitals must therefore be energetically closer to the Rh−Rh σ and π fragment orbitals than to the same orbitals in the molybdenum system. This result is consistent with the greater inherent stability of Rh d orbitals compared to Mo d orbitals. There is thus more ligand character introduced into these Rh−Rh orbitals than into the analogous Mo−Mo orbitals. As for $Mo_2(O_2CCH_3)_4$, there is no C−F antibonding character to destabilize the a_{1g} and e_u acetate fragment orbitals. The Mo−Mo σ and π bonds might therefore be expected to mix even less well with these ligand fragment orbitals than is suggested by our calculations.

Conclusions

The photoelectron data reported here provide new insight into the nature of the metal−metal and metal−ligand valence electronic interactions in the general class of $M_2(O_2CR)_4$ molecules. These data for $Rh_2(O_2CCF_3)_4$ are the first for a Rh−Rh system in this class, and this information reflects on the understanding of the electron distribution and bonding between metal atoms in the group VI dimetal tetracarboxylates. The ionizations of $Rh_2(O_2CCF_3)_4$ support a ground-state configuration of $\sigma^2\pi^4\delta^2\delta^{*2}\pi^{*4}$ with nearly degenerate ionizations from the Rh−Rh δ^* and π^* orbitals. The δ ionization precedes a band that contains the σ and π ionizations. The enhancement of δ ionizations observed in the He II experiment for other dimetal systems is present again in the spectrum of $Rh_2(O_2CCF_3)_4$ and assists in assigning this ionization. This phenomenon is traced to the high ligand character present in the Rh−Rh σ- and π-containing orbitals of lowest binding energy.

Computations help to reveal the orbital interactions that are important in determining the electronic structure of these molecules, but the methods exhibit varying degrees of success in accounting quantitatively for these experimental observations. The characters of the molecular orbitals are sensitive to the relative energies of the metal−metal and ligand fragment orbitals, and the characters can change substantially with ionization. Overall, the ADF method is reasonable in calculating the order and relative separation of metal−metal orbitals in $Rh_2(O_2CCF_3)_4$. The ionization energies determined by the ΔE_{SCF} method are in good agreement with experiment. Even the Koopmans values, with the exception of that for the ligand-based Rh−Rh σ ionization, match the order and relative separation of the valence ionizations despite their neglect of the electron relaxation process that occurs upon ionization. This finding underscores the extent of the metal−ligand orbital mixing and the influence of these interactions on the properties of these systems.

The increased ligand character in the σ and π orbitals of the molecules with perfluoroacetate ligands is interesting in light of the high electron-withdrawing ability of the fluorine atoms and the stabilization of the ligand orbitals. The photoelectron spectra show that the metal−metal ionizations are stabilized similar to the ligand ionizations, and thus the electron withdrawal by the fluorine atoms affects the entire molecule and does not preferentially stabilize the ligand orbitals relative to the metal orbitals. A critical factor in these systems is the overlap of the filled fluorine p orbital "lone pairs" with the C−C bond in one of the highest occupied orbitals of the ligand. As shown by each of the calculational methods reported here, this intraligand interaction destabilizes this particular ligand orbital relative to other orbitals and allows a better energy match between this orbital and the M−M σ and π bonds. As a consequence, the σ and π bond orbitals of $Mo_2(O_2CCF_3)_4$ are associated with more ligand character than are those of $Mo_2(O_2CCH_3)_4$ or $Mo_2(O_2CH)_4$. The σ and π bond orbitals of $Rh_2(O_2CCF_3)_4$ contain the largest amount of ligand character of this group of molecules because of the combination of the fluorine electronic effects and the greater inherent stability of the rhodium d orbitals. The significant amount of ligand character introduced into these molecular orbitals is demonstrated experimentally by photoelectron spectroscopy.

Acknowledgment. D.L.L. acknowledges support by the National Science Foundation (Grant No. CHE9618900) for studies of metal-metal bonding, the U.S. Department of Energy (Division of Chemical Sciences, Office of Basic Energy Science, Office of Energy Research, DE-FG03-95ER14574) and the Materials Characterization Program, Department of Chemistry, University of Arizona. M.A.L. thanks the National Science Foundation for a predoctoral fellowship. F.A.C. also thanks the National Science Foundation for support.

JA993618L